FEATURE ARTICLE

Frequency Selected Ultrafast Infrared Vibrational Echo Studies of Liquids, Glasses, and Proteins

K. A. Merchant,[†] Qing-Hua Xu,[†] David E. Thompson,[†,‡] and M. D. Fayer*

Department of Chemistry, Stanford University, Stanford, California 94305

Received: May 8, 2002; In Final Form: June 27, 2002

Ultrafast infrared frequency selected vibrational echo (FSVE) experiments are used to study temperature-dependent dynamic interactions in liquids, glasses, and proteins. Vibrational echo experiments measure vibrational dephasing. In general, the large bandwidths associated with ultrashort IR pulses will excite multiple vibrational transitions of a molecular system. In addition to the 0−1 transition of a particular mode of interest, the 1−2 transition, other modes, combination bands, and modes of other species can be excited. A one-dimensional vibrational echo experiment involving multiple transitions can be difficult to address theoretically. By selecting the proper detection wavelengths (a frequency slice through a 2D time-frequency vibrational echo), FSVE makes it possible to effectively isolate a two state system (in terms of the dynamical experimental observables) from within a complex multistate system. First, the FSVE method is used to study the dynamics of CO stretching mode of RuTPPCOPy (TPP = 5,10,15,20-tetraphenylporphyrin, Py = pyridine) in two solvents: poly(methyl methacrylate) (PMMA) and 2-methyltetrahydrofuran (2-MTHF). The results demonstrate the fundamental difference in the influence of a glassy and a liquid solvent on vibrational dephasing. In PMMA, a glass at all temperatures studied, the dephasing rate is linear in temperature. In 2-MTHF, the dephasing is linear for temperatures below T_g, but it changes form, becoming very steep slightly above T_g. Calculations using a model frequency−frequency correlation function (FFCF) show that the different temperature dependences in PMMA and 2-MTHF can be modeled in a unified manner, with at least two solvent motions contributing to the dephasing in liquids, that is, inertial and diffusive motions. FSVE is then applied to the study of the dynamics of the protein myoglobin in water by observing the vibrational dephasing of the stretching mode of CO bound to the active site of myoglobin (Mb-CO). The A_1 and A_3 conformational substates of Mb-CO are found to have different dephasing rates with different temperature dependences. A frequency−frequency correlation function derived from molecular dynamics simulations of Mb-CO at 298 K is used to calculate the vibrational echo decay. The calculated decay shows substantial agreement with the experimentally measured decays. The FSVE experiment probes protein dynamics and provides an observable that can be used to test structural assignments for the Mb-CO conformational substates.

I. Introduction

In this article, we describe the application of ultrafast infrared frequency selected vibrational echo (FSVE) experiments to the study of dynamics of condensed matter molecular systems. The energy of a vibrational oscillator is exceedingly sensitive to dynamical fluctuations of its structural environment. For a solute molecule in a liquid or glassy solvent, the environment is the surrounding solvent. For a molecular oscillator associated with a particular functional group of a protein, the environment is the surrounding protein. The sensitivity is manifested by time dependent variations in the vibrational transition frequency. In principle, information on the time evolution of vibrational transition frequencies can be obtained from vibrational absorption line shapes.[1−3] However, in complex condensed matter systems, the line shape is frequently dominated by static or quasistatic variations in the oscillator's environment, which give rise to inhomogeneous line broadening. Thus, dynamical information is masked in a linear absorption experiment.

Vibrational echo experiments are capable of revealing underlying dynamical information by eliminating inhomogeneous broadening of vibrational absorption lines.[4−9] However, the ultrashort infrared (IR) pulses necessary to study vibrational dephasing have bandwidths that can exceed the anharmonicity of the vibrational transition, and the frequency separations between different vibrational modes, combination bands, and the modes of distinct molecular species.[10−12] Frequency selected vibrational echo experiments simplify the study of vibrational dynamics by making it possible to observe the dephasing dynamics of a single vibrational transition without sacrificing time resolution.[10,11,13,14] Effectively, a multilevel system can be studied as if it is a two-level system, making it possible to perform a more detailed analysis of the data.[13]

* To whom correspondence should be addressed.
[†] K. A. M., Q.-H. X., and D. E. T. contributed equally to this work.
[‡] Permanent address: Department of Chemistry, Lawrence University, Appleton, WI 54912.

10.1021/jp021145q CCC: $22.00
Published on Web 08/27/2002

Photon echoes,[15,16] which probe electronic transitions, and other visible optical nonlinear experiments have benefited from the recent rapid developments and applications of ultrashort optical pulses.[17] However, ultrafast resonant nonlinear experiments involving electronic transitions are complicated by molecular vibrations that give rise to vibrational progressions in the electronic absorption spectrum.[18−20] Intramolecular vibrational modes have a significant influence on the third-order nonlinear signals. The complexity brought on by the simultaneous excitation of many vibronic transitions can make it difficult to analyze the results of ultrafast nonlinear electronic transition experiments.[18−20]

Vibrational echoes avoid the problems associated with electronic transition experiments by examining dynamical interactions on the ground electronic state potential surface and by measuring the dephasing of a particular vibrational degree of freedom.[4−9,17,21] Even in the simplest situation in which the pulse bandwidth spans a single vibrational mode, the system is still multilevel because the vibration is an anharmonic quantum oscillator, that is, in addition to the 0−1 transition, the 1−2 transition can be involved. Interferences among different excitation pathways in a 1D vibrational echo experiment that occur in a multilevel quantum oscillator system will produce a vibrational echo decay that is not a single exponential and that can display anharmonic beats, even if the individual transition's (0−1 transition and 1−2 transition) dynamic dephasing is exponential.[10,11,14,22] If the individual decays are intrinsically nonexponential, then the 1D signal is virtually impossible to separate into its components.

By spectrally resolving the vibrational echo signal, 2D vibrational echo spectroscopy can provide information that cannot be obtained from a 1D experiment.[7,8,12,14,23−26] However, in many applications, what is desired is the equivalent of a 1D experiment that is free from the complications that arise from a multilevel system. It is useful to be able to reduce a multistate system into what is effectively a two-state system because a great deal of theoretical work is based on a single transition between two quantum levels.[1,9,27]

In the following, recent examples of the application of FSVE experiments are presented.[12,13,28,29] In the first set of experiments, the stretching mode of CO bound to a metalloporphyrin compound, RuTPPCOPy (TPP = 5,10,15,20-tetraphenylporphyrin, Py = pyridine), in two solvents, poly(methyl methacrylate) (PMMA) and 2-methyltetrahydrofuran (2-MTHF), is studied. 1D experiments are presented that display a nonexponential decay with oscillations at the frequency of the anharmonic shift. FSVE experiments are then performed at several wavelengths. It is shown that the vibrational dephasing of the 0−1 transition can be obtained without interference from the 1−2 transition. The temperature dependences of the dephasing in the two solvents are then discussed. In PMMA, which is a glass at all temperatures studied, the temperature dependence is linear in T. However, in 2-MTHF, a substantial change in the temperature dependence of the pure dephasing is observed upon passing through the glass transition. A model is proposed to explain the data that involves multiple time scales for the solvent modulation of the vibrational transition frequency. Detailed calculations provide a rationalization for the observations in terms of both inertial and diffusive components of the solvent dynamics.

In addition, investigations of the dynamics of the protein myoglobin using FSVE and 2D vibrational echoes are described.[12] Protein dynamics have been the focus of intense theoretical and experimental study for over 25 years. In particular, a tremendous amount of work has focused on myoglobin, which is a small globular protein involved in the storage of oxygen. Over 50 years ago, sperm whale myoglobin was the first protein to be characterized structurally with X-ray crystallography,[30] and continued refinements of protein structures from X-ray[31,32] and neutron scattering[33] have yielded structures with atomic resolution. From a functional standpoint, the reversible binding of small molecule ligands, such as O_2, CO, and NO, represents one of the simplest chemical actions of a protein. Because of its relatively small size, structural calculations and molecular dynamics simulations on myoglobin are tractable with modern computers and algorithms.[34−38] These factors make myoglobin an ideal system to test ideas about protein dynamics, structure, and function.

In the studies presented below, the stretching mode of CO bound to the active site of myoglobin (Mb-CO) is probed. Previous vibrational echo experiments on Mb-CO were performed mainly at low temperatures using relatively long pulses (~1 ps).[39−46] The application of ultrafast FSVE and 2D vibrational echo experiments permit a more detailed examination of Mb-CO dynamics at biologically relevant temperatures. The dynamical time scales relevant to vibrational echoes in Mb-CO are readily accessed in a molecular dynamics simulation.[34,36,38,47] The simulations provide the frequency−frequency correlation function (FFCF), which is then used to calculate the vibrational echo observable.[12] The results are in substantial agreement with the vibrational echo data, despite the absence of adjustable parameters in the comparison. The combination of molecular dynamics simulations and ultrafast infrared vibrational dynamics studies represents a powerful new approach to understanding and testing detailed models of protein dynamics and structure.

II. Experimental Procedure and Theoretical Background

The apparatus for the ultrafast infrared vibrational echo experiments has been described in detail previously.[10,13] Briefly, tunable femtosecond mid-IR pulses with a repetition rate of 1 kHz were generated by an optical parametric amplifier pumped with a regeneratively amplified Ti:sapphire laser. A 15%/85% ZnSe beam splitter was used to create a weak beam (wave vector $\mathbf{k}_1$) and strong beam (wave vector $\mathbf{k}_2$). The weak beam was delayed with respect to the strong beam by a stepper−motor translation stage. The beams were crossed and focused at the sample to a spot size of 150 μm. The vibrational echo pulse was generated in the phase-matched direction, $-\mathbf{k}_1 + 2\mathbf{k}_2$ (see Figure 1a). The vibrational echo signal was passed through a monochromator to select the proper observation wavelength, and the signal was measured with a liquid-nitrogen-cooled HgCdTe detector. IR pump−probe experiments were also performed ($\boldsymbol{k}_2$ pump and $\boldsymbol{k}_1$ probe) to determine the vibrational lifetime, and the pump−probe signal was also dispersed through the monochromator (set to the 0−1 transition frequency) before detection to obtain the lifetime of the desired transition and to suppress scattered light. The resolution of the monochromator was set to 2 cm^{-1}. The pulse energy was ~3.5 μJ/pulse (before the beam splitter).

RuTPPCO (see Figure 1b), PMMA, methylene chloride (CH_2Cl_2), and 2-MTHF were purchased from Aldrich. The RuTPPCOPy/2-MTHF solution was prepared by dissolving the RuTPPCO in 2-MTHF and then adding 2-fold molar excess of pyridine. Pyridine is the fifth ligand on the Ru (see Figure 1b). The optical density (OD) of the CO stretching mode in the 200 μm path length sample cell was 0.1. The PMMA glass film was prepared by mixing PMMA with a RuTPPCOPy/CH_2Cl_2 solution. The solution was spread on a clean glass plate and

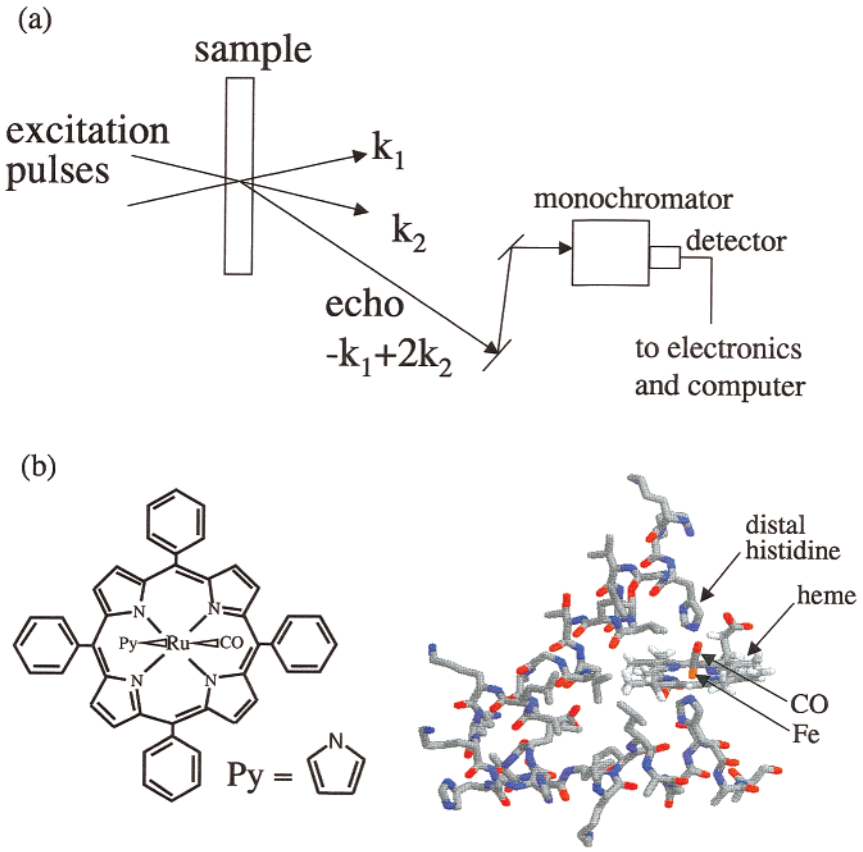

Figure 1. (a) Schematic of the frequency-selected vibrational echo (FSVE) experiment. (b) Chemical structures of RuTPPCOPy and Mb-CO near the heme pocket.

dried under a closed atmosphere for 2 days. The sample was then placed under vacuum for a week to remove the remaining solvent. The thickness of the PMMA film sample was 150−200 μm, and the OD was ∼0.5 at the absorption maximum. The samples were placed between two CaF_2 windows in a copper sample cell.

Horse heart myoglobin (Sigma Corp., St. Louis, MO) was dissolved in pH 7, 0.1 M phosphate buffer, centrifuged to remove large particulates, and then purged with nitrogen to remove dissolved oxygen. The myoglobin solution was reduced with excess dithionite solution and stirred under a CO atmosphere for 1 h before being filtered with a 0.45 μm acetate filter and placed in a custom gastight 50 μm copper sample cell with CaF_2 windows. A small portion of the structure of Mb-CO is shown in Figure 1b. The temperatures of both types of samples were controlled with a continuous flow cryostat and monitored with a silicon diode temperature sensor bonded to one of the CaF_2 windows.

The vibrational echo signals can be calculated in terms of the response function. The procedures have been presented in detail in the monograph by Mukamel.[9] Here only a very brief description is given. The homodyne third-order vibrational echo signal, detected by a slow detector, is given by

$$S(\tau) \propto \int_0^\infty |P^{(3)}(\tau, t)|^2 \, dt \qquad (1)$$

where the third-order polarization $P^{(3)}$ is the convolution of the total response function R with the three electric fields that interact with the sample (one interaction with the first pulse and two interactions with the second pulse). τ is the delay between the pulses. $R = \sum_i R_i$ contains contributions from different dynamical processes and different time-ordered terms, which can be represented by double-sided Feynman diagrams.[9,48−50] The R_i can be calculated from a function, $g(t)$. $g(t)$ is obtained from the frequency-frequency correlation function (FFCF) $\langle \delta\omega_{10}(\tau_2)\delta\omega_{10}(0)\rangle$

$$g(t) = \int_0^t d\tau_1 \int_0^{\tau_1} d\tau_2 \, \langle \delta\omega_{10}(\tau_2)\delta\omega_{10}(0)\rangle \qquad (2)$$

The FFCF provides the connection between the physical processes occurring in the sample and the vibrational echo experimental observable. Through the FFCF, detailed models of the nature of the temperature-dependent dynamical processes that produce vibrational dephasing can be tested.

For positive delay times, only two terms contribute to the vibrational echo signal for a two-level system. $R = R_1 + R_2 = 2\exp[-2g(\tau) - 2g(t) + g(\tau + t)]$, where R_1 and R_2 denote the contributions from pathways (diagrams) that after the second interaction with the radiation field place the system in the ground and excited state, respectively. In this formula, the contribution from the vibrational Stokes shift (originating from the imaginary part of $g(t)$) is reasonably assumed to be negligibly small, and therefore, $R_1 = R_2$. For a three-level system (the $|0\rangle$, $|1\rangle$, and $|2\rangle$ states of the vibrational oscillator), an additional contribution from R_3 needs to be included: $R_3 = -2R_1 e^{i\Delta t}$, where Δ is the anharmonic shift, that is, the difference in frequency between the 0−1 transition and the 1−2 transition (see Figure 2b).[11,22,51] R_3 involves the excitation of the 1−2 transition after the first two interactions with the radiation field place the oscillator in the first excited vibrational state ($v = 1$). T_1, the vibrational lifetime contribution to the vibrational dephasing, can be included in the response function R by multiplying R with the population relaxation contribution: $\exp[-(t + \tau)/2T_{1,v=1}]$ for the R_1 and R_2 terms, and $\exp[-(\tau/2T_{1,v=1}) - t/(1/2T_{1,v=1} +$

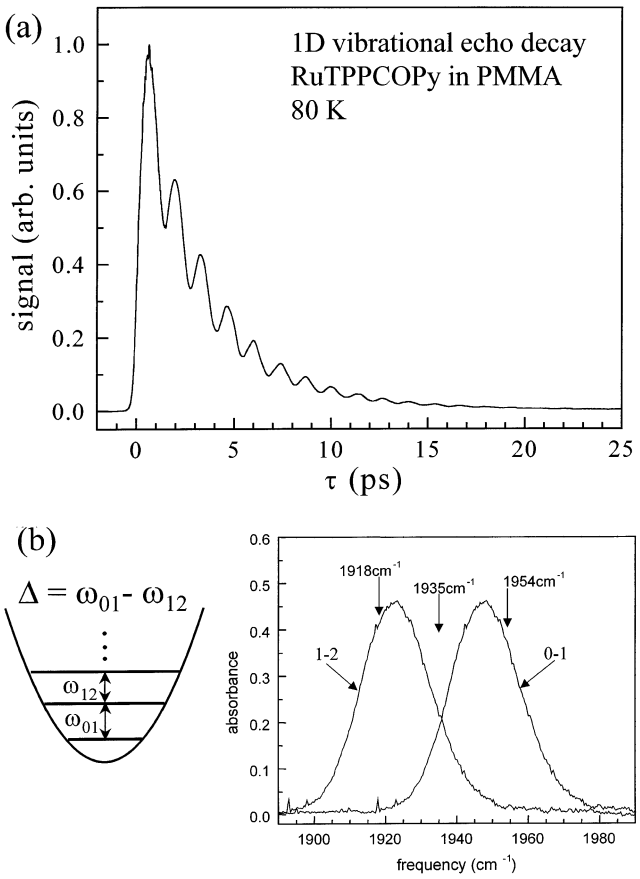

Figure 2. (a) 1D vibrational echo data for the CO stretching mode of RuTPPCOPy in PMMA at 80 K. The decay is multiexponential with anharmonic beats. (b) The absorption spectrum of RuTPPCOPy in PMMA at 80 K labeled 0−1. The curve labeled 1−2 is a model of the 1−2 absorption spectrum obtained by shifting the 0−1 spectrum by the anharmonic shift of the 1−2 transition, which was determined from the beat frequency in (a). The frequencies indicated with arrows correspond to the observation frequencies of the data presented in Figure 3. The anharmonic shift, Δ, is illustrated with a schematic of an oscillator potential energy surface.

$1/2T_{1,\upsilon=2})$] for the R_3 term. For some samples, the FSVE decays are single exponentials characterized by a total dephasing time, T_2. For exponential decays, the lifetime contribution can be removed from the data using $1/T_2 = 1/T_2^* + 1/2T_1$, where T_2^* is the vibrational pure dephasing, that is, dephasing caused by frequency fluctuations of the vibrational transition. Diagrams with time orderings that do not lead to rephasing and only contribute to the signal at negative delay times and around $\tau = 0$ have been discussed thoroughly in the literature,[9,13,52,53] and the discussions will not be recapitulated here. However, all necessary diagrams have been included in the data analysis.[12,13] Inclusion of all diagrams is necessary when the shape of the vibrational echo decay curve is of interest.[9]

III. Vibrational Dynamics in Liquid and Glassy Solvents

Figure 2a displays 1D vibrational echo decay data for RuTPPCOPy in PMMA at 80 K.[13] The decay of the 1D signal is multiexponential and is strongly modulated by oscillatory beats. Figure 2b displays the 0−1 spectrum and a representation of the 1−2 spectrum.[13] The 1−2 spectrum was modeled as the 0−1 spectrum shifted by the anharmonicity, which was determined from the beat frequency.[11,22,51] It is assumed that the line widths are the same for the two transitions. In this system, as shown in Figure 2b, the inhomogeneous broadening (∼22 cm^{-1})

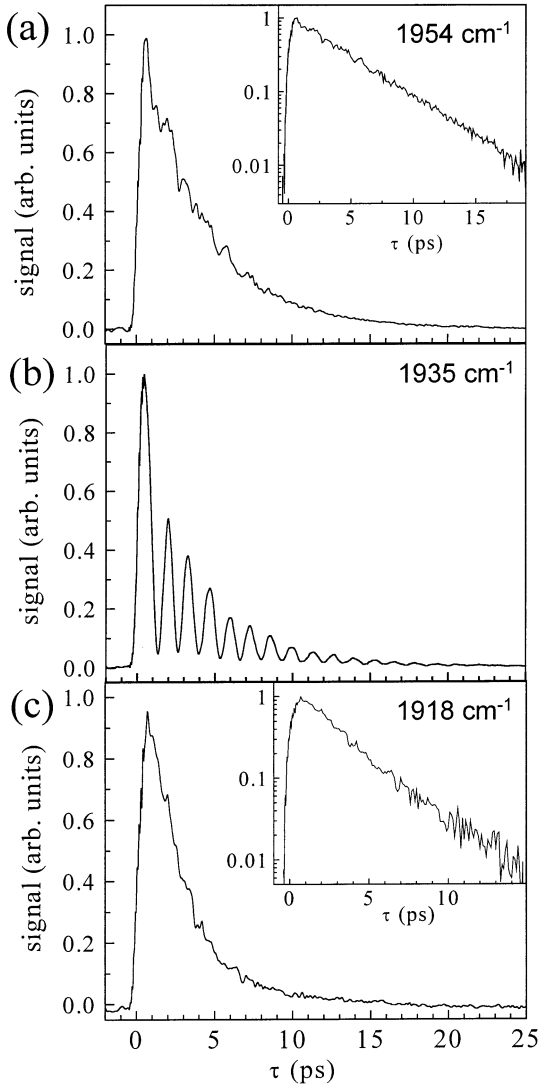

Figure 3. Frequency-selected vibrational echo decays of the CO stretch of RuTPPCOPy in PMMA at 80 K. (a) 1954 cm^{-1}, the 0−1 transition. (b) 1935 cm^{-1}, between the 0−1 and 1−2 transitions. (c) 1918 cm^{-1}, the 1−2 transition. The wavelengths are indicated with arrows in Figure 2. Almost 100% modulation is seen at 1935 cm^{-1}, where the 0−1 and 1−2 spectra overlap (see Figure 2). At the other two frequencies, single exponential decays (see insets) are observed.

is comparable to the vibrational anharmonicity (∼25 cm^{-1}). When there is spectral overlap of 0−1 and 1−2 transitions, the interference of the R_1/R_2 (two level diagrams involving only two levels $\upsilon = 0$ and 1) with R_3 (three level diagram involving $\upsilon = 0$, 1, and 2) produces a beat at the difference frequency between the 0−1 and 1−2 transitions (the anharmonic shift)[11,22,51] which is illustrated in Figure 2b. Such beats are referred to as anharmonic beats.[11,22,51] Even if the decays associated with R_1/R_2 and R_3 terms are individually distinct single exponentials, the interference of these terms will cause the total signal to be a triexponential with beats. The time constants associated with the individual terms are difficult to resolve, especially when the time constants are similar. If the individual decays are nonexponential and the functional form is not known, then it is virtually impossible to separate the distinct decay components.

The problems associated with the 1D decay (Figure 2) can be overcome by performing FSVE experiments. By selecting the proper detection wavelengths, it is possible to obtain the signal corresponding solely to the R_1/R_2 terms (0−1 transition) or to the R_3 term. Figure 3 displays FSVE data for three different

detection wavelengths, 1954, 1935, and 1918 cm^{-1} (see Figure 2b).[13] The data in Figure 3a were taken slightly on the blue side of the center of the 0−1 transition (1954 cm^{-1}); the data in 3b were taken halfway between the two transitions (1935 cm^{-1}); and the data in 4c were taken slightly on red side of the 1−2 transition (1918 cm^{-1}). In Figure 3b, the beats are very pronounced with almost 100% modulation depth. In this case, both R_1/R_2 and R_3 terms contribute to the signal, producing strong anharmonic beats. When the blue wavelength is selected (Figure 3a), only the R_1/R_2 terms contribute to the signal. The decay shown in Figure 3a (1954 cm^{-1}) is the pure 0−1 transition, two level vibrational echo decay.[11] When the red wavelength (1935 cm^{-1}, Figure 3c) is selected, only the R_3 term contributes to the signal. At both 1954, and 1918 cm^{-1}, the oscillations are virtually eliminated, and the vibrational echo decays can be fit with single exponentials, as shown in the insets.

The decay rate associated with R_3 (Figure 3c) is faster than that of R_1/R_2 (Figure 3a).[13] The fact that a single-exponential vibrational echo decay is obtained suggests that the underlying vibrational dynamics can be well separated into homogeneous and inhomogeneous broadening components. The vibrational echo decay time of 4 ps for the 0−1 transition (R_1/R_2 terms) gives a dynamic line width of 0.65 cm^{-1} assuming the absorption line is inhomogeneously broadened. This line width is much narrower than the absorption line width (∼22.8 cm^{-1}), showing that the absorption line is indeed massively inhomogeneously broadened. In this situation, the dynamics can be described in terms of a Bloch description. In the Bloch picture, the decay rates of the signal associated with R_1 and R_2 terms are identical and are denoted by $4\gamma_{01}$, whereas the decay rate associated with the R_3 term is $(2\gamma_{01} + 2\gamma_{12})$, where γ_{01} and γ_{12} denote the total dephasing rates associated with the 0−1 and 1−2 transitions, respectively. The data demonstrate that the total dephasing rate associated with the 1−2 transition is faster than that of the 0−1 transition, that is, $\gamma_{01} = 1/(16\ ps)$ and $\gamma_{12} = 1/(7\ ps)$ at 80 K.

The total dephasing process has contributions from both vibrational population relaxation and pure dephasing processes. For a harmonic oscillator, the lifetime of a vibrational level is inversely proportional to its quantum number, whereas the pure dephasing is only dependent on the difference between the quantum numbers of the levels involved.[54] For a system with a small anharmonicity, it is reasonable to assume that the pure dephasing rates associated with 0−1 and 1−2 transitions are very similar. The dephasing rates of the two transitions were shown to be identical at elevated temperatures in liquid 2-MTHF, where the lifetime contribution is negligible.[13] At low temperature, the vibrational population decays of the levels make a significant contribution to the total dephasing.[51,55] Therefore, the difference in the total dephasing rates in the current situation is most likely due to the shorter vibrational lifetime of the $v = 2$ level than that of the $v = 1$ level where v is the vibrational quantum number.[51] The lifetime of the $v = 1$ level measured by a pump−probe experiment is 12.6 ps at 80 K, which yields a pure dephasing rate of ∼1/(44 ps) for the 0−1 transition. By assuming the identical pure dephasing rates for the 0−1 and 1−2 transitions, the lifetime of the $v = 2$ level is estimated to be 6.2 ps. The ratio of the lifetimes of the two vibrational levels, $T_{1,v=1}/T_{1,v=2}$, is 2.05, very close to 2.0 predicted for a harmonic oscillator.[54]

By using FSVE, it is possible to examine the temperature-dependent dephasing of the CO stretching mode 0−1 transition of RuTPPCOPy, a two state system. The temperature dependences of the dephasing in the two solvents, PMMA and 2-MTHF, are very different. In PMMA, in the temperature range 60−300 K, all of the vibrational echo decays can be fit very well as single exponentials.[29] If the system is in the inhomogeneous broadening limit, then the total dephasing rate is four times the vibrational echo decay rate, yielding a dephasing time T_2. Assuming T_2 can be obtained in this manner, the resulting dynamical line width ($1/\pi T_2$) is much narrower than the absorption line width at all temperatures, which confirms the assumption that the system is in the inhomogeneous limit. The lifetime contribution (T_1) to the dephasing was removed to obtain the pure dephasing. The vibrational lifetime in both solvents slightly increases with the increasing temperature, ranging from 12 to 17 ps in the temperature range studied.[29]

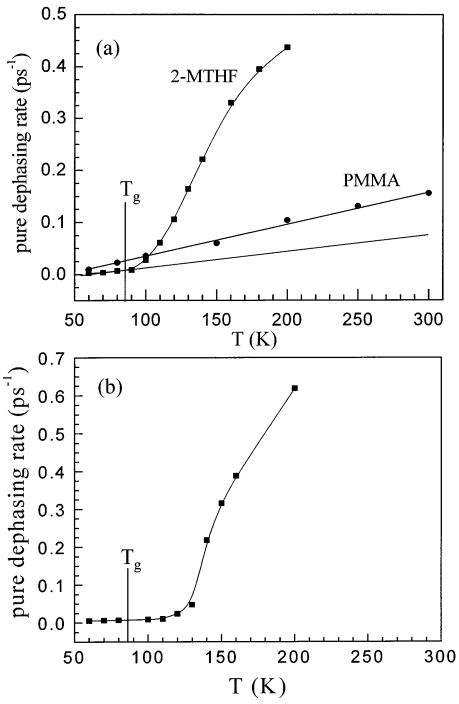

Figure 4. (a) Temperature-dependent pure dephasing rates of the CO stretching mode of RuTPPCOPy in 2-MTHF (squares) and PMMA (circles). The data taken in PMMA are linear in temperature as shown by the line through the points. In 2-MTHF, below T_g to ∼10 K above T_g (T_g = 86 K), the data are also linear. At ∼10 K above T_g, the 2-MTHF liquid data become nonlinear and rise steeply. The curve through the squares is an aid to the eye. (b) Model calculations of the pure dephasing rate of the CO stretching mode of RuTPPCOPy in 2-MTHF. The calculations were performed using eqs 4 and 5. The calculations reproduce the essential features of the data but agreement is not quantitative. The calculations are linear in temperature at low temperatures and then rise steeply in the same manner as the data. However, the break from linearity occurs ∼30 K above T_g, in contrast to the data that has its break ∼10 K above T_g.

The vibrational echo decays in 2-MTHF are single exponentials only at low temperature and become more and more nonexponential with increasing temperatures.[29] The dephasing time is extracted by fitting the vibrational echo profiles with a single exponential from 60 to 200 K. The vibrational echo decay profiles for temperatures above 200 K are strongly nonexponential, and therefore, only the temperature dependence of data for 200 K and below will be discussed.

The pure dephasing rates in the two solvents are plotted as a function of temperature in Figure 4a.[29] The pure dephasing rate in PMMA (circles) increases linearly with increasing temperature over the full temperature range as is evident from the line drawn through the circles. At the lowest temperatures, the data in 2-MTHF (squares) appear to increase linearly with temper-

ature. The line through the lowest temperature points is an aid to the eye. However, as the temperature continues to increase, the data rise very steeply. The curve drawn through the squares is, again, an aid to the eye. At sufficiently high temperature, the increase becomes somewhat slower. The apparent break in the temperature dependence, from linear to steeply rising nonlinear, occurs just above $T_g = 86$ K. At the lowest temperatures, where both solvents are glasses, the pure dephasing rates in 2-MTHF are somewhat slower than those in PMMA, and the apparent linear temperature dependence is less steep (see Figure 4a). Thus, the homogeneous line widths in 2-MTHF are slightly narrower and increase less rapidly compared to the homogeneous line widths in PMMA in the glassy solvents. In contrast, as the temperature is raised above the 2-MTHF T_g, the dephasing rates in 2-MTHF become much faster than those in PMMA. This fundamental difference in the temperature dependence of the dephasing rates that occurs above T_g suggests that an additional dephasing mechanism becomes active when the solvent goes from a solid to a liquid.

The viscosity of liquids changes dramatically as the temperature is raised above T_g. For a fragile glass forming liquid[56,57] such as 2-MTHF, the viscosity as a function of temperature can often be described by a Vogel−Tamman−Fulcher (VTF) equation.[58−60] A VTF temperature dependence is steeper than exponentially activated near T_g. Experiments have shown that changes in solvent viscosity can affect vibrational dephasing.[46,61,62] The steep increase in the dephasing rate with increasing temperature observed in 2-MTHF liquid may be associated, at least in part, with the temperature dependence of the viscosity as well as the overall temperature change.

First consider vibrational dephasing in glassy solvents. Even in a solid glassy matrix, there are still solvent dynamics. Two types of dynamics can occur. One type is the structural rearrangements that occur in glasses even at low temperatures.[63−65] The second type is phonon-induced dynamics, the so-called "inertial motions". Here we will assume that the inertial motions are responsible for the homogeneous dephasing. The assumption is supported by the qualitative agreement between the data and the calculations[29] discussed below. Future work using stimulated vibrational echo experiments will provide additional information on which mechanism is operative.

Vibrational and electronic transitions of probe molecules in solvents share similar solute−solvent interactions. The broad electronic and vibrational absorption line shapes in condensed phases are both due to transition frequencies modulated by solvent structural fluctuations. The transition frequency modulation can be described in terms of a frequency-frequency correlation function (FFCF).[29]

In a glass, a simple model for the FFCF can be written as

$$\langle \delta\omega_{10}(t)\delta\omega_{10}(0)\rangle = \Delta_h^2(T)\exp(-t/\tau_h) + \Delta_{in}^2 \qquad (3)$$

where Δ_h is the range of frequencies sampled by the fluctuations that give rise to the homogeneous dephasing, and τ_h is the time scale characterizing the fluctuations. Δ_h reflects the change in energy associated with fluctuations about an essentially fixed local structure. Like phonons in a crystal lattice, heat will cause displacements of the positions and orientations of the solvent molecules without changing the local structure about which the fluctuations occur. Δ_{in} is the spread in frequencies that gives rise to the inhomogeneous broadening. Δ_{in} is caused by the wide variety of local solvent structures in a glass that remain essentially fixed, even on very long time scales. Because the local structures in a glass are essentially static below T_g, Δ_{in} is assumed to be temperature independent below T_g. In the motional narrowing limit, the pure dephasing rate $1/T_2^* = \Delta_h^2\tau_h$. T_2^* is obtained from the vibrational echo decay by removing the lifetime contribution, T_1. The vibrational echo decay and pure dephasing rates are insensitive to the Δ_{in} when Δ_{in} is much larger than $\Delta_h^2\tau_h$. Both the multimode Brownian oscillator (MBO) model[9,17,66] and the viscoelastic model[67−70] predict that the fluctuation magnitude squared, Δ^2, is proportional to the temperature.[9,69] In the high-temperature limit, $\Delta^2 = 2kT/\hbar\lambda$,[9] where λ, the reorganization energy, is assumed to be independent of temperature. Using this form for $\Delta_h^2(T)$, the linear temperature dependences of the dephasing rates observed in both PMMA and 2-MTHF below their glass transition temperatures suggest that τ_h is insensitive to the temperature change. The above model also predicts that the slope of the dephasing rate vs T at low temperatures is proportional to λ. Differences in λ would account for the fact that the homogeneous line widths in 2-MTHF are narrower and increase less rapidly than those in PMMA at low temperatures (comparing the slopes of two straight lines in Figure 4a). A temperature independent τ_h is consistent with results obtained by Nagasawa et al.,[66] which show that the time scale of the inertial motion in PMMA at low and high temperatures (30 and 300 K) are very similar. Therefore, the linear temperature dependences of the vibrational pure dephasing rates observed in PMMA and 2-MTHF glasses are consistent with the proposition that the homogeneous dephasing is phonon-induced; that is, ultrafast inertial motions are responsible for the homogeneous dephasing in the high-temperature glasses.

Although glasses undergo structural evolution to some extent, the nature of structural dynamics is fundamentally different in solvents such as 2-MTHF when the temperature is raised above T_g where they become liquids. In comparison to glasses, liquids have greater compressibility and a much stronger change in density with temperature. Of particular importance here is that, as the temperature is raised above T_g, diffusive motions of the solvent molecules occur on faster and faster time scales. Solvent molecules can reorganize to accommodate changes in the properties of a solute, such as a change in dipole moment, associated with vibrational excitation. In addition to phonon-induced dephasing, solvent diffusive motions provide a dephasing mechanism that does not exist in a glass. Therefore, at least two different types of motions, occurring on different time scales, can contribute to the pure dephasing in liquids. Δ_{in} of eq 3 no longer reflects a purely static contribution to the absorption spectrum. To replicate the diffusive dynamics associated with the solvent structure that is essentially static in the glass, a modified FFCF is used:[29]

$$\langle \delta\omega_{10}(t)\delta\omega_{10}(0)\rangle = \Delta_h^2(T)\exp(-t/\tau_h) + \Delta_{in}^2(T)\exp(-t/\tau_d) \qquad (4)$$

where τ_d is the time associated with the diffusive dynamics and $\Delta_{in}^2(T)$ is temperature dependent in the liquid. This formula reduces to eq 3 as $\tau_d \rightarrow \infty$, that is, below T_g, where Δ_{in}^2 is also assume to be temperature independent.

The temperature dependence of the diffusive motions is different from that of the inertial motion. The fluctuation magnitude squared, Δ_{in}^2, is assumed to be proportional to the temperature.[9,69] In addition, the correlation time, τ_d, is expected to become shorter as the temperature increases. The temperature affects τ_d through the solvent viscosity η. Different theoretical models have predicted $\tau_d \propto \eta$.[61,69] This differs from the inertial part of the correlation function where it is assumed that only Δ_h^2 is dependent on temperature. The temperature dependences of Δ_{in} and τ_d will significantly affect the dephasing rate.

Model calculations were performed based on the following inputs.[29] Δ_h^2 and Δ_{in}^2 were obtained using the 80 K data as a reference. At 80 K, the vibrational echo decay is exponential. A value of $\tau_h = 100$ fs is a typical value.[69,71] This value is assumed to hold here and, as discussed above, is also assumed to be temperature independent. Using this value, the vibrational echo decay and the linear absorption spectrum was fit to give $\Delta_h = 0.265$ ps^{-1} and $\Delta_{in} = 0.95$ ps^{-1}. The viscosities of 2-MTHF as a function of temperature were obtained from interpolation of the viscosity data.[72] For the model calculation, the constant relating the linear dependence of τ_d on η[46,61] is assumed to be similar to water; that is, viscosities of 10^1-10^6 cP correspond to the correlation times of 2 ps to 200 ns.[46,61] Using these correlation times as a function of viscosity and the 2-MTHF viscosities, the correlation times at different temperatures were determined.[29] With these inputs, the temperature-dependent FFCF in 2-MTHF is given by

$$\langle \delta\omega_{10}(t)\delta\omega_{10}(0)\rangle = (0.265 \text{ ps}^{-1})^2\left(\frac{T}{80}\right)\exp(-t/\tau_h) + (0.95 \text{ ps}^{-1})^2\left(\frac{T}{80}\right)\exp\left[-t/\left(\frac{\eta \times 2 \text{ ps}}{10 \text{ cP}}\right)\right] \quad (5)$$

The calculations of the vibrational echo decays using eq 5 for the FFCF show that the decays are single exponentials at low temperatures and become nonexponential at high temperatures, in accord with experimental observations.[29]

Figure 4b displays the calculated temperature-dependent pure dephasing rates.[29] Of principal importance here is the fact that many of the qualitative features of the experimentally observed temperature dependence are reproduced. At the lowest temperatures, the pure dephasing rate increases linearly with temperature. In a calculation for the PMMA solvent, eq 3 is used, and the temperature dependence does not deviate from linearity because Δ_{in}^2 is frozen and acts as static inhomogeneity. However, for 2-MTHF, modeled with the FFCF given in eq 5, the diffusive motion is not frozen, and the dephasing and vibrational echo decay rates are very sensitive to the increase in the value of Δ_{in}, especially when the τ_d becomes fast. Above T_g, the calculated temperature dependence of the pure dephasing rate becomes nonlinear, and the rate of pure dephasing increases very rapidly. At sufficiently high temperatures (not investigated here), τ_d will become so fast that the dephasing arising from diffusive motions will also be in the motional narrowing limit ($\Delta_{in}\tau_d < 1$). A pure dephasing rate of $\Delta_h^2\tau_h + \Delta_{in}^2\tau_d$ will be obtained, and the vibrational echo decay rate will be $2/T_2$ rather than $4/T_2$, the decay rate for an inhomogeneously broadened system. The corresponding absorption spectrum will be Lorentzian. The reduction in the rate of increase of the dephasing rate with temperature at high temperature is partially due to the transition from the inhomogeneous broadening limit to the homogeneous broadening limit.

Although the calculations based on the FFCF given in eqs 4 and 5 capture the main features of the data with no adjustable parameters, the agreement is not quantitative. The focus here is on the vibrational echo decays, but the FFCF can also be used to calculate the linear absorption spectrum. The FFCF shows a mild increase of the width of the absorption spectrum with temperature, which is greater than that seen experimentally. Of particular importance is the fact that the vibrational echo data in 2-MTHF begin to deviate from linearity and rise steeply <10 K above T_g. In contrast, the calculations do not begin to deviate from linearity and rise steeply until ~30 K above T_g. The calculated steep increase in the pure dephasing rate with temperature above T_g is also somewhat too steep, and by 200 K it is ~40% greater than the data value. The actual difference in the magnitude of the pure dephasing is likely due to the use of the relationship between τ_d and η based on the approximate values for water. However, the use of a scaling factor between τ_d and η other than the one obtained for water cannot account for the late onset of the steep rise in the calculated curve. The simulations show that using the FFCF in the form of eq 5, the amplitude of Δ_{in} has no effect on the total dephasing rate when τ_d is very slow (slower than 1 ns, which is likely for temperatures around T_g). However, a possible rapid change of Δ_h or τ_h just above T_g would have a large effect on the total dephasing rates and might be responsible for the early onset of the steep temperature dependence observed in the experimental data.[29]

In the model embodied in eqs 4 and 5, passage through T_g was accounted for by the addition of the viscosity-dependent diffusive dephasing term, $\exp(-t/\tau_d)$ and the temperature dependence of Δ_{in}. The parameters other than τ_d were set based on the homogeneous dephasing and the absorption line shape below T_g. However, when the solvent passes through T_g from below, there is an abrupt increase in its compressibility.[73] This change could be manifested in an increase in Δ_h.[69] In addition, the "softening" of the solvent as it goes above T_g could cause a change in the "phonon" modes of the solvent, which may well influence the time scale of the inertial response of the system. The temperature (viscosity) dependence of the time constant of the diffusive motion appears to be at least in part responsible for the activation of the dephasing process above T_g observed in 2-MTHF. However, the early onset of rapid dephasing just above T_g suggests that there are additional contributions not contained in the change in viscosity with temperature.

IV. Protein Dynamics−Vibrational Dephasing of the CO Stretch of Mb-CO

The infrared absorption spectrum of the CO stretch of horse heart Mb-CO shows that Mb-CO exists in at least three spectroscopically distinct conformational substates: the A_0 state centered at ~1965 cm^{-1}, the A_1 state at ~1944 cm^{-1}, and the A_3 state at ~1932 cm^{-1} (the initial proposal for the existence of an A_2 state has fallen out of fashion).[74−78] These substates are thought to correspond to different interconverting structures of the protein, possibly with different biological function. The interconversion rates are too fast to be resolved using NMR[74] but are essentially static on the vibrational echo time scale. Various hypotheses for the structural identities of these substates have recently been reviewed.[38]

Early one-dimensional vibrational echo experiments have been applied extensively to the study of Mb-CO.[39−46] The experiments were performed using laser pulses with a duration of ~1 ps and bandwidth of ~15 cm^{-1} tuned to the A_1 substate. These experiments were conducted mainly at low temperatures where the vibrational dephasing is comparatively slow. Therefore, relatively long pulses with correspondingly narrow bandwidths could be employed. Such pulses could be tuned into the A_1 line with little spectral overlap of the other conformational substates. However, in low viscosity solvents such as water, the dephasing is very fast. At biologically relevant temperatures, the 1D vibrational echo decay shapes measured with the ~1 ps pulses were strongly influenced by the pulse duration and contained substantial contributions from the A_3 substate.

Here the results of experiments using FSVE and 2D vibrational echoes permit the A_1 and A_3 substates of horse heart Mb-CO to be studied separately with high time and frequency

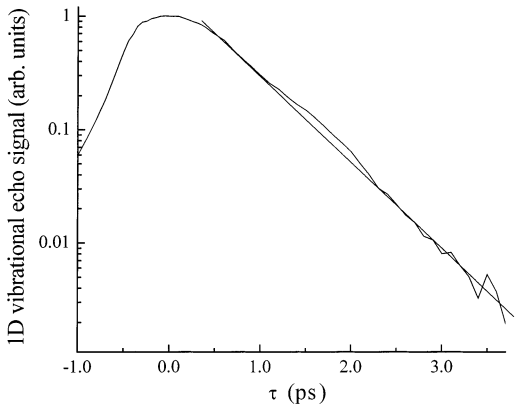

Figure 5. 1D vibrational echo decay at 298 K. The decay appears exponential, that is, it is linear on the semilog plot. The oscillations in the data are real, see text.

resolution.[12] The A_3 substate vibrational echo decay is more rapid than the A_1 substate decay and shows a weak temperature dependence. The A_1 vibrational echo decay shows a more pronounced dependence on temperature. Both decay curves are nonexponential.

Ultrafast one-dimensional vibrational echo decays of the CO stretch of Mb-CO in water were measured at 279, 298, and 323 K.[12] The vibrational echo decay at 298 K is shown in Figure 5. The vibrational echo decay appears exponential over 3 decades of signal decay. (There are deviations from a straight line in the data that are real oscillations produced by anharmonic beats as seen in Figure 2a.[11,14]) In principle, the decay contains a contribution from pure dephasing and from the vibrational lifetime (T_1 = 16.5 ps).[12] In all of the experiments discussed below, the time scale of pure dephasing is much faster than the vibrational lifetime, T_1.[44] Therefore, T_1 does not contribute significantly to the vibrational echo observables.

Because the bandwidth of the laser pulses used in the 1D experiments presented here is ~100 cm^{-1}, the 1D decays have contributions from all three A substates. In addition, the laser bandwidth exceeds the CO stretch anharmonicity of 25 cm^{-1}, resulting in signal contributions from 1−2 vibrational transitions. The 1D vibrational echo decay shown in Figure 5 has, in principle, six contributions, that is, contributions from the 0−1 transitions of the A_0, A_1, and A_3 substates and contributions from the 1−2 transitions of each of these substates. It is possible that each of these six transitions will give rise to a distinct decay. The signal is observed at the intensity level, which is the squared modulus of the polarization. The signal is not only comprised of six decays, it also has cross terms between the various decays. Thus, the seemingly simple 1D decay is a superposition of many decays.

Frequency selected vibrational echo spectroscopy and 2D vibrational echoes makes it possible to resolve these various contributions into their individual components and measure each one separately. The background-subtracted linear absorption spectrum for horse heart Mb-CO is shown in Figure 6a. Figure 6b shows the results of fitting the absorption spectrum to three bands, A_0, A_1, and A_3 (solid lines). The fit was performed using three Voigt line shapes[12] and the approximate known center frequencies of the three bands.[74−77] The Voigt line shape is used as an approximation to the true absorption line shape that is neither Gaussian nor Lorentzian. The 1−2 vibrational bands (dashed lines) for each substate are also shown in Figure 6b because they contribute to the vibrational echo signal.[11,12] The 1−2 bands were obtained by displacing the 0−1 bands by the measured anharmonicity of 25.4 cm^{-1}.[51] Recent measurements

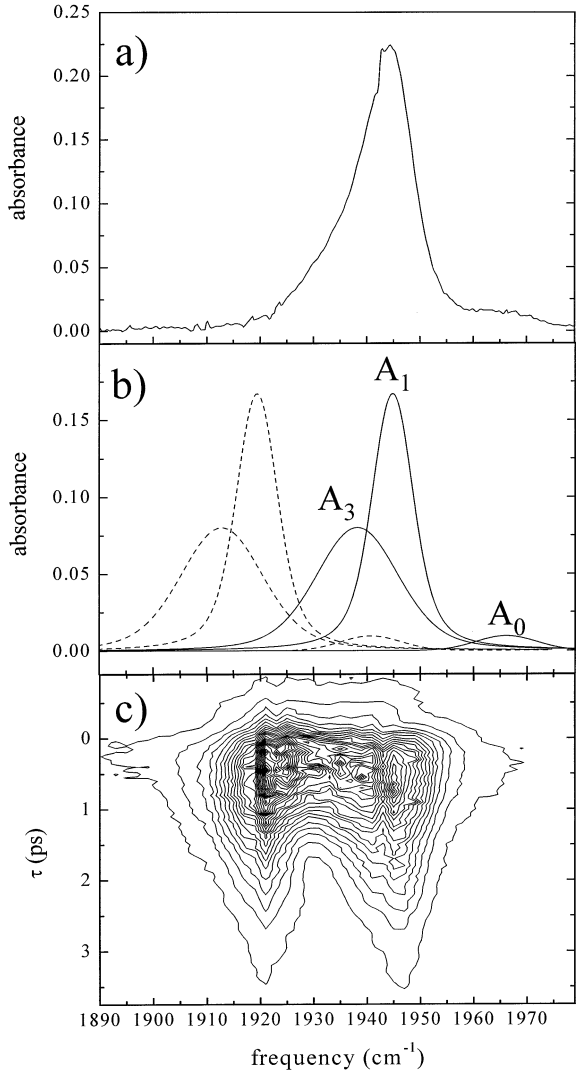

Figure 6. (a) Background-subtracted linear-infrared absorption spectrum of the CO stretch of Mb-CO. (b) Three bands used to fit the absorption spectrum corresponding to the A_0, A_1, and A_3 substates (solid lines). The excited-state absorption for each band is also shown as a peak shifted to lower energy from the fundamental transition frequency by the anharmonicity of the CO stretch (dotted lines). (c) A contour plot of the 2D vibrational echo spectrum of Mb-CO. The vibrational echo decay rate is frequency dependent, reflecting different decay rates for the A_1 and A_3 substates. At 1946 cm^{-1}, the decay is predominantly A_1. At 1931 cm^{-1}, the decay is predominantly A_3. The 0−1 and 1−2 dephasing rates for each substate are the same within experimental error.

using 2D vibrational echo spectroscopy show that the line widths of the A_1 0−1 and 1−2 bands are the same within experimental error. It is assumed that for the A_0 and A_3 transitions the 0−1 and 1−2 line widths are also the same.

The full 2D time-frequency vibrational echo spectrum was recorded at 298 K and is shown as a contour plot in Figure 6c. It is clear that different spectral components of the Mb-CO spectrum have different decay rates. The six bands in Figure 6b each represent individual contributions to the 1D vibrational echo decay. At this pH, the A_0 band is minimally populated, and it is not discernible in the data presented in Figure 6c. The 0−1 and 1−2 transitions of the A_1 substate appear at ~1944 and ~1920 cm^{-1}, respectively. The two transitions have the same decay rate within experimental error. The decay curve is nonexponential and has a decay constant (1/e value) of ~700 fs. Because the CO vibrational transition in Mb-CO is not highly anharmonic, it is not surprising that the 1−2 level has a similar

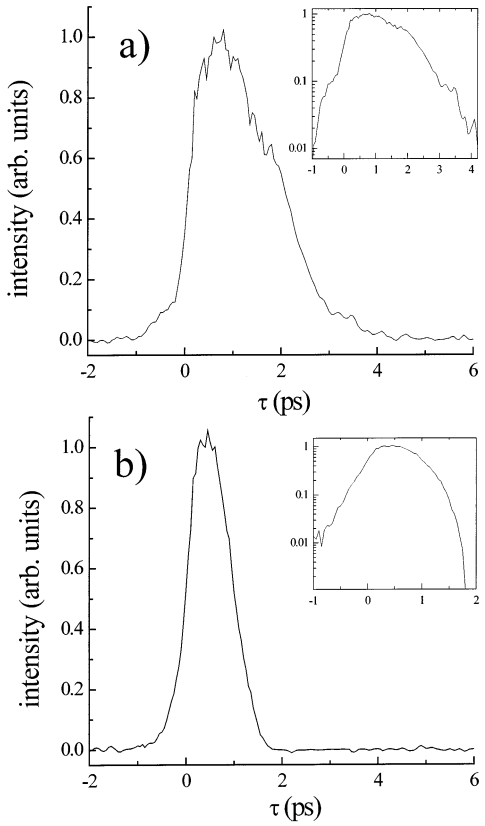

Figure 7. Vibrational echo decays at (a) 1946 cm^{-1} and (b) 1932 cm^{-1} of Mb-CO at 298 K. Contributions from overlapping lines have been removed by subtracting off interfering signal contributions at the polarization level. The vibrational echo signal at 1932 cm^{-1} decays much more rapidly than the echo signal at 1946 cm^{-1}. The functional form of the echo decay appears to be different for the two wavelengths. The insets show the decays on semilog plots. Both echo decay curves are nonexponential.

dephasing rate as the 0−1 level. The 0−1 and 1−2 vibrational echo decays of the A_3 substates are also equal to each other within experimental error. The vibrational lifetimes of the A_1 and A_3 substates at 298 K (16.5 and 14.8 ps, respectively) make a negligible contribution to the overall dephasing rate. The A_3 substate vibrational echo signal (contours around 1932 cm^{-1}) decays more rapidly than the A_1 substate (contours around 1946 cm^{-1}).

Figure 7 displays FSVE decays that are predominantly the A_1 0−1 decay and the A_3 0−1 decay. The A_1 decay (Figure 7a) was obtained by taking a slice through the data at 1946 cm^{-1}. At 1946 cm^{-1}, the 0−1 and 1−2 A_0 transitions make a negligible contribution to the vibrational echo signal (see Figure 6b). However, the 0−1 A_3 transition makes a small contribution to the signal. The curve in Figure 7a was obtained by subtracting the contribution from the A_3 line at the polarization level.[12] The procedure for removing small contributions from other lines has been described in detail.[12] The inset shows the decay on a semilog plot. The vibrational echo decay at this wavelength is nonexponential. An analogous procedure was performed at 1932 cm^{-1} to reduce unwanted contributions from the A_1 line. The vibrational echo decay curve at 1932 cm^{-1} is highly nonexponential (see semilog inset). Thus, 2D vibrational echo spectroscopy makes it possible to obtain the dephasing dynamics of the individual substates with reduced interference from the decays of other transitions even when there is some spectral overlap. It is clear from comparison of the shapes of the curves in Figure 7 parts a and b that the dephasing dynamics at the two detection frequencies are very different.

The vibrational echo decays at the two wavelengths used for Figure 7 were measured at 279 and 320 K in addition to the room-temperature measurements.[12] The signal contributions from the individual substates were isolated at the two detection wavelengths with the same procedure performed on the data in Figure 7. The data at 1946 cm^{-1} shows an appreciable increase in the dephasing rate as the temperature increases. However, the data at 1932 cm^{-1} shows a much weaker dependence of the dephasing rate on the temperature over the same temperature range.

A comparison of the 1D vibrational echo data (Figure 5) and 2D vibrational echo data (Figure 7) at 298 K clearly shows that the multidimensional vibrational echo technique provides dynamical information that is not obtainable from 1D vibrational echo measurements. In fact, the 1D decays measured with broad bandwidth pulses can be misleading because, in general, they are a composite of many different decays that can have distinct functional forms and temperature dependences. It is interesting and important to note that the interpretation of the vibrational echo data changes dramatically from the 1D to the 2D scans. The apparent exponential decay of the 1D data implies an extremely rapid decay of the FFCF and motional narrowing of the Mb-CO dynamic spectral line by the protein's dynamics. However, the 1D vibrational echo data is deceptive because the nonexponential form of the 2D data indicates that a different type of FFCF offers a more reasonable description of the vibrational echo data.[62] The fact that the different conformational substates of Mb-CO have different nonexponential dephasing rates was hidden in the 1D experiment. Rector et al.[46] have shown that a distribution of nonexponential vibrational echo decay rates can lead to the appearance of an overall exponential decay in a 1D vibrational echo scan. Frequency resolving the vibrational echo signal allows the dynamics of the individual substates to be examined separately and permits a closer examination of the dephasing processes that occur in Mb-CO.

The vibrational echo data suggest that the A_1 and A_3 substates have different dephasing rates at room temperature, and that the dephasing rates of the two lines have distinct temperature dependences.[12] Despite numerous spectroscopic and computational studies,[32,38,47,74,76,78−80] the structural origins of the A substates in Mb-CO remain controversial. In particular, the protonation state of the distal histidine His64 (see Figure 1), the proximity and orientation of this residue to the CO ligand, and the absence or presence of a hydrogen bond between the ligand and this residue have all been proposed by various studies to give rise to the different substates. A recent high-resolution crystal structure of Mb-CO[32] and several recent computational studies[38,80] have suggested that N_ϵ is protonated, in contrast to the conclusions of previous X-ray[31] and neutron scattering[33] data. Recent simulations of Mb-CO[47] have also employed the tautomer with protonated N_δ. The A_0 substate is generally thought to correspond to the imidazole ring of His64 being rotated away from the heme pocket, although the protonation state at neutral or high pH is unclear. The origins of the A_1 and A_3 substates are subject to a greater degree of speculation.[47,80]

The different dephasing dynamics of the A_1 and A_3 substates determined by 2D vibrational echo measurements must reflect the structural differences between these states. Williams et al. have recently used molecular dynamics simulations to compute the classical FFCF for sperm whale Mb-CO in water at 298 K.[35] The frequency fluctuations are assumed to arise from a dynamic Stark effect in which the instantaneous electric field

produced at the ligand by its surroundings results in a transient shift in the vibrational frequency of CO.[41,46] The electrostatic interaction between the ligand and its surroundings is represented by the coupling of the electric dipole of CO to $\vec{E}(t)$, the total electric field from protein and solvent at the midpoint of the CO bond. Park et al. have determined $\Delta\mu \approx 0.14$ D for CO in a variety of Mb mutants and other heme containing compounds.[81] $\Delta\mu$ is the coupling constant between the fluctuating electric field and CO vibrational transition frequency. Williams et al. have employed this value of $\Delta\mu$ together with molecular dynamics simulations of the fluctuating electric field at the ligand in Mb-CO to compute the FFCF.[12,35]

In agreement with previous simulations of heme pocket dynamics in Mb-CO,[47] the imidazole of His64 (the distal histidine) assumed configurations with a relatively large distance from the ligand, which were assumed to correspond to substate A_0, and configurations in which the imidazole was much closer to the CO, which were assumed to correspond to A_1/A_3. Also, in common with prior simulations,[38] no separate identification of A_1 and A_3 substates was possible with the δ nitrogen protonated. (Recent simulations with the ϵ nitrogen protonated do show distinct substates, which may correspond to A_1 and A_3.[82]) The decay of the FFCF for A_1/A_3 was dominated at short times (<400 fs) by dynamics of His64, which were uncorrelated from dynamics of the rest of the protein and the water solvent. On longer time scales (<30 ps), the FFCF reflected correlated dynamics of the rest of the protein and of the water. The A_1/A_3 FFCF obtained from the simulation was fit to the functional form of a biexponential decay plus a constant. The constant, as in eq 3, reflects slowly varying protein structures that do not contribute to dynamics on the experimental time scale. Then, the FFCF is given by[12,35]

$$\langle \delta\omega(t)\delta\omega(0)\rangle = \Delta_1^2 \exp(-t/\tau_1) + \Delta_2^2 \exp(-t/\tau_2) + \Delta_0^2 \quad (6)$$

with $\Delta_1 = 2.07$ ps^{-1}, $\Delta_2 = 1.14$ ps^{-1}, $\Delta_0 = 0.67$ ps^{-1}, $\tau_1 = 0.14$ ps, and $\tau_2 = 4.95$ ps.

The functional form for the FFCF given in eq 6 was employed to calculate the vibrational echo signal, including the effects of laser pulse shapes. The finite duration laser pulse shape and all necessary diagrams were included in the calculation. The resulting vibrational echo signal is shown by the solid curves in Figure 8, in which it is compared to the experimental 1946 cm^{-1} data (dashed curve) in Figure 8a and to the experimental 1932 cm^{-1} data (dashed curve) in Figure 8b. The simulated signal decays more rapidly than either measured signal, but it is closer to that of the 1932 cm^{-1} vibrational echo decay. Figure 8 represents a rigorous comparison of calculation and experiment, because *no adjustable parameters have been employed*. The simulation results show qualitative agreement with both signals. Although the agreement is not quantitative, the comparison between simulations and experiments with no adjustable parameters shows that it is possible to test models of protein structure and dynamics through the comparison of frequency selected vibrational echo experiments and simulations. Recent simulations with the ϵ nitrogen of the distal histidine protonated show two distinct structures that have dynamics that give rise to different FFCFs and calculated vibrational echo decay curves.[83] The preliminary results indicate much better agreement between the simulations/vibrational echo calculations and the data. These results may permit the identification of the A_1 and A_3 substate structures.[83]

The debate in the literature over the structural origins of the A_1 and A_3 conformational substates is over 20 years old. One reason for this is that the only calculation that could be done to test a hypothesis for the structural origins of the substates was to compute a vibrational frequency. The 2D vibrational echo provides new information for assessing the accuracy of computational studies of protein dynamics. Proposed structures can be tested not only by whether they produce the correct trends in vibrational frequency but also by whether they give rise to the correct relative dephasing rates and temperature dependences. The added dimension of agreement with dynamical data as well as structural data can provide additional rigor for computational studies that seek a molecular understanding of proteins.

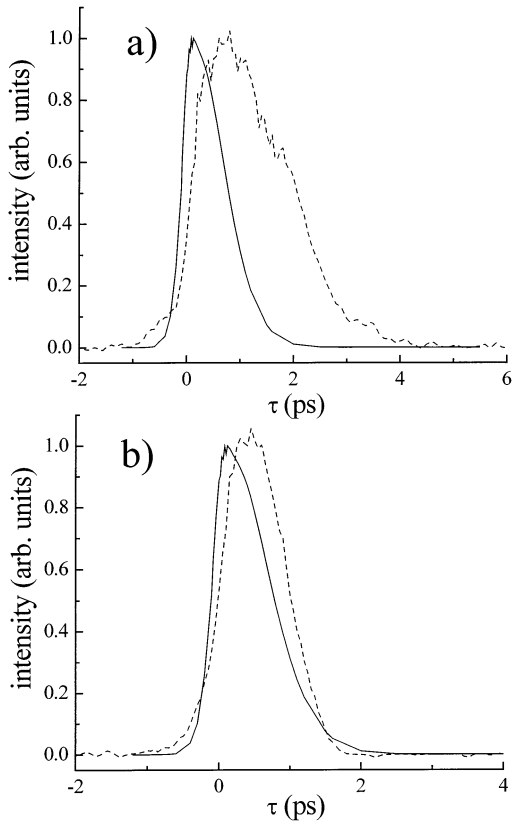

Figure 8. Comparison between the calculated vibrational echo decay (solid lines) calculated with the FFCF of the A_1/A_3 state of Mb-CO derived from molecular dynamics simulations and the measured 1946 cm^{-1} (dashed line in 7a) and 1932 cm^{-1} (dashed line in 7b) vibrational echo decays. The calculation has no adjustable parameters.

V. Concluding Remarks

In this article, we have demonstrated the utility of the FSVE technique for the study of dynamic molecular interactions through the observation of vibrational dephasing. Experiments have been used to investigate liquids, glasses, and proteins. By selecting the proper detection wavelengths, FSVE experiments permit the independent detection of the dephasing dynamics associated with 0−1 and 1−2 vibrational transitions, eliminating cross terms and anharmonic beats that occur in conventional 1D vibrational echo signals for anharmonic vibrational systems. In systems in which multiple vibrational modes are excited by the broad bandwidth associated with an ultrashort IR excitation pulse, FSVE enables particular transitions to be isolated and studied. FSVE also permits the examination of a single species in a multicomponent molecular system. FSVE is useful whenever there is a spectroscopic window in which the number of transitions that contribute to a 1D vibrational echo is reduced.

Multidimensional vibrational echo techniques such as FSVE can reveal a variety of information about vibrational dynamics

that is not obtainable from either the absorption spectrum or 1D vibrational echo techniques. The development and application of ultrafast multidimensional infrared vibrational echo techniques are just beginning. These methods, which permit the observation of the structural evolution and dynamic intermolecular interactions of molecular systems, are providing a fundamentally new approach to the study of chemical, biological, and materials problems.

Acknowledgment. This work was supported by the National Institutes of Health (1R01-GM61137) and the National Science Foundation (DMR-0088942). K.A.M. was partially supported by an Abbott Laboratories Stanford Graduate Fellowship. We thank Prof. Roger Loring and his group for performing the MD simulations on MbCO.

References and Notes

(1) Gordon, R. G. *J. Chem. Phys.* **1965**, *43*, 1307.
(2) Gordon, R. G. *J. Chem. Phys.* **1965**, *42*, 3658.
(3) Gordon, R. G. *Adv. Magn. Reson.* **1968**, *3*, 1.
(4) Zimdars, D.; Tokmakoff, A.; Chen, S.; Greenfield, S. R.; Fayer, M. D.; Smith, T. I.; Schwettman, H. A. *Phys. Rev. Lett.* **1993**, *70*, 2718.
(5) Tokmakoff, A.; Fayer, M. D. *J. Chem. Phys.* **1995**, *103*, 2810.
(6) Rector, K. D.; Fayer, M. D. *Int. Rev. Phys. Chem.* **1998**, *17*, 261.
(7) Asplund, M. C.; Lim, M.; Hochstrasser, R. M. *Chem. Phys. Lett.* **2000**, *323*, 269.
(8) Zanni, M. T.; Asplund, M. C.; Hochstrasser, R. M. *J. Chem. Phys.* **2001**, *114*, 4579.
(9) Mukamel, S. *Principles of Nonlinear Optical Spectroscopy*; Oxford University Press: New York, 1995.
(10) Thompson, D. E.; Merchant, K. A.; Fayer, M. D. *J. Chem. Phys.* **2001**, *115*, 317.
(11) Merchant, K. A.; Thompson, D. E.; Fayer, M. D. *Phys. Rev. A* **2002**, *65*, 23817.
(12) Merchant, K. A.; Thompson, D. E.; Xu, Q.-H.; Williams, R. B.; Loring, R. F.; Fayer, M. D. *Biophys. J.* **2002**, *82*, 3277.
(13) Xu, Q.-H.; Thompson, D. E.; Merchant, K. A.; Fayer, M. D. *Chem. Phys. Lett.* **2002**, *355*, 139.
(14) Merchant, K. A.; Thompson, D. E.; Fayer, M. D. *Phys. Rev. Lett.* **2001**, *86*, 3899.
(15) Kurnit, N. A.; Abella, I. D.; Hartmann, S. R. *Phys Rev. Lett.* **1964**, *13*, 567.
(16) Abella, I. D.; Kurnit, N. A.; Hartmann, S. R. *Phys. Rev.* **1966**, *14*, 391.
(17) Rullière, C. *Femtosecond laser pulses: principles and experiments*; Springer: New York, 1998.
(18) Book, L. D.; Scherer, N. F. *J. Chem. Phys.* **1999**, *111*, 792.
(19) Larsen, D. S.; Ohta, K.; Xu, Q. H.; Cyrier, M.; Fleming, G. R. *J. Chem. Phys.* **2001**, *114*, 8008.
(20) Ohta, K.; Larsen, D. S.; Yang, M.; Fleming, G. R. *J. Chem. Phys.* **2001**, *114*, 8020.
(21) *Ultrafast Infrared and Raman Spectroscopy*; Fayer, M. D., Ed.; Marcel Dekker: New York, 2001; Vol. 26.
(22) Tokmakoff, A.; Kwok, A. S.; Urdahl, R. S.; Francis, R. S.; Fayer, M. D. *Chem. Phys. Lett.* **1995**, *234*, 289.
(23) Golonzka, O.; Khalil, M.; Demirdoven, N.; Tokmakoff, A. *Phys. Rev. Lett.* **2001**, *86*, 2154.
(24) Khalil, M.; Tokmakoff, A. *Chem. Phys.* **2001**, *266*, 213.
(25) Demirdoven, N.; Khalil, M.; Golonzka, O.; Tokmakoff, A. *J. Phys. Chem. A* **2001**, *105*, 8030.
(26) Zanni, M. T.; Gnanakaran, S.; Stenger, J.; Hochstrasser, R. M. *J. Phys. Chem. B* **2001**, *105*, 6520.
(27) Kubo, R. A Stochastic Theory of Line-Shape and Relaxation. In *Fluctuation, Relaxation and Resonance in Magnetic Systems*; Ter Haar, D., Ed.; Oliver and Boyd: London, 1961.
(28) Xu, Q.-H.; Fayer, M. D. *Laser Phys.* **2002**, accepted.
(29) Xu, Q.-H.; Fayer, M. D. *J. Chem. Phys.* **2002**, *117*, 2732.
(30) Kendrew, J. C. *Acta Crystallogr.* **1948**, *1*, 336.
(31) Kuriyan, J. W.; Karplus, M.; Petsko, G. A. *J. Mol. Biol.* **1986**, *192*, 133.
(32) Vojtechovsky, J.; Chu, K.; Berendzen, J.; Sweet, R. M.; Schlichting, I. *Biophys. J.* **1999**, *77*, 2153.
(33) Cheng, X.; Schoenborn, B. P. *J. Mol. Biol.* **1991**, *220*, 381.
(34) Elber, R.; Karplus, M. *Science* **1987**, *235*, 318.
(35) Williams, R. B.; Loring, R. F.; Fayer, M. D. *J. Phys. Chem. B* **2001**, *105*, 4068.
(36) Meller, J.; Elber, R. *Biophys. J.* **1998**, *74*, 789.
(37) Sagnella, D. E.; Straub, J. E.; Thirumalai, D.; Jackson, T. A.; Anfinrud, P. A. *Proc. Natl. Acad. Sci. U.S.A.* **1999**, *96*, 14324.
(38) Rovira, C.; Schulze, B.; Eichinger, M.; Evanseck, J. D.; Parrinello, M. *Biophys. J.* **2001**, *81*, 435.
(39) Rella, C. W.; Rector, K. D.; Kwok, A. S.; Hill, J. R.; Schwettman, H. A.; Dlott, D. D.; Fayer, M. D. *J. Phys. Chem.* **1996**, *100*, 15620.
(40) Rella, C. W.; Kwok, A.; Rector, K. D.; Hill, J. R.; Schwettmann, H. A.; Dlott, D. D.; Fayer, M. D. *Phys. Rev. Lett.* **1996**, *77*, 1648.
(41) Rector, K. D.; Rella, C. W.; Kwok, A. S.; Hill, J. R.; Sligar, S. G.; Chien, E. Y. P.; Dlott, D. D.; Fayer, M. D. *J. Phys. Chem. B* **1997**, *101*, 1468.
(42) Rector, K. D.; Engholm, J. R.; Hill, J. R.; Myers, D. J.; Hu, R.; Boxer, S. G.; Dlott, D. D.; Fayer, M. D. *J. Phys. Chem. B* **1998**, *102*, 331.
(43) Rector, K. D.; Engholm, J. R.; Rella, C. W.; Hill, J. R.; Dlott, D. D.; Fayer, M. D. *J. Phys. Chem. A* **1999**, *103*, 2381.
(44) Rector, K. D.; Fayer, M. D. *Laser Chem.* **1999**, *19*, 19.
(45) Rector, K. D.; Thompson, D. E.; Merchant, K.; Fayer, M. D. *Chem. Phys. Lett.* **2000**, *316*, 122.
(46) Rector, K. D.; Jiang, J.; Berg, M.; Fayer, M. D. *J. Phys. Chem. B* **2001**, *105*, 1081.
(47) Schulze, B. G.; Evanseck, J. D. *J. Am. Chem. Soc.* **1999**, *121*, 6444.
(48) Joo, T.; Jia, Y.; Yu, J. Y.; Lang, M. J.; Fleming, G. R. *J. Chem. Phys.* **1996**, *104*, 6089.
(49) Xu, Q. H.; Scholes, G. D.; Yang, M.; Fleming, G. R. *J. Phys. Chem. A* **1999**, *103*, 10348.
(50) Xu, Q. H.; Fleming, G. R. *J. Phys. Chem. A* **2001**, *105*, 10187.
(51) Rector, K. D.; Kwok, A. S.; Ferrante, C.; Tokmakoff, A.; Rella, C. W.; Fayer, M. D. *J. Chem. Phys.* **1997**, *106*, 10027.
(52) Hamm, P.; Lim, M.; Hochstrasser, R. M. *Phys. Rev. Lett.* **1998**, *81*, 5326.
(53) Fourkas, J. T. *Laser Phys.* **1995**, *5*, 661.
(54) Fourkas, J. T.; Kawashima, H.; Nelson, K. A. *J. Chem. Phys.* **1995**, *103*, 4393.
(55) Rector, K. D.; Fayer, M. D. *J. Chem. Phys.* **1998**, *108*, 1794.
(56) Boehmer, R.; Nagi, K. L.; Angell, C. A.; Plazek, D. J. *J. Chem. Phys.* **1993**, *99*, 4201.
(57) Huang, D.; Mckenna, G. B. *J. Chem. Phys.* **2001**, *114*, 5621.
(58) Angell, C. A. *J. Phys. Chem. Solids* **1988**, *49*, 863.
(59) Angell, C. A.; Smith, D. L. *J. Phys. Chem.* **1982**, *86*, 3845.
(60) Fredrickson, G. H. *Annu. Rev. Phys. Chem.* **1988**, *39*, 149.
(61) Fayer, M. D. *Annu. Rev. Phys. Chem.* **2001**, *52*, 315.
(62) Berg, M. A.; Rector, K. D.; Fayer, M. D. *J. Chem. Phys.* **2000**, *113*, 3233.
(63) Phillips, W. A. *J. Low Temp. Phys.* **1972**, *7*, 351.
(64) Anderson, P. W.; Halperin, B. I.; Varma, C. M. *Philos. Mag.* **1972**, *25*, 1.
(65) Fourkas, J. T.; Kivelson, D.; Mohanty, U.; Nelson, K. A. *Supercooled liquids: advances and novel applications*; American Chemical Society: Washington, DC, 1997.
(66) Nagasawa, Y.; Passino, S. A.; Joo, T.; Fleming, G. R. *J. Chem. Phys.* **1997**, *106*, 4840.
(67) Berg, M. *Chem. Phys. Lett.* **1994**, *228*, 317.
(68) Berg, M. *J. Phys. Chem.* **1998**, *102*, 17.
(69) Berg, M. A.; Hubble, H. W. *Chem. Phys.* **1998**, *233*, 257.
(70) Berg, M. A. *J. Chem. Phys.* **1999**, *110*, 8577.
(71) Passino, S. A.; Nagasawa, Y.; Joo, T.; Fleming, G. R. *J. Phys. Chem. A* **1997**, *101*, 725.
(72) Tokmakoff, A., Thesis, Stanford University, Stanford, CA, 1994.
(73) Stillinger, F. H.; Debenedetti, P. G.; Sastry, S. *J. Chem. Phys.* **1998**, *109*, 3983.
(74) Caughey, W. S.; Shimada, H.; Choc, M. C.; Tucker, M. P. *Proc. Natl. Acad. Sci. U.S.A.* **1981**, *78*, 2903.
(75) Shimada, H.; Caughey, W. S. *J. Biol. Chem.* **1982**, *257*, 1893.
(76) Hong, M. K.; Draunstein, D.; Cowen, B. R.; Frauenfelder, H.; Iben, I. E. T.; Mourant, J. R.; Ormos, P.; Scholl, R.; Schulte, A.; Steinbach, P. J.; Xie, A.; Young, R. D. *Biophys. J.* **1990**, *58*, 429.
(77) Johnson, J. B.; Lamb, D. C.; Frauenfelder, H.; Muller, J. D.; McMahon, B.; Nienhaus, G. U.; Young, R. D. *Biophys. J.* **1996**, *71*, 1563.
(78) Müller, J. D.; McMahon, B. H.; Chen, E. Y. T.; Sligar, S. G.; Nienhaus, G. U. *Biophys. J.* **1999**, *77*, 1036.
(79) Oldfield, E.; Guo, K.; Augspurger, J. D.; Dykstra, C. E. *J. Am. Chem. Soc.* **1991**, *113*, 7537.
(80) Phillips, G. N., Jr.; Teodoro, M. L.; Li, T.; Smith, B.; Olson, J. S. *J. Phys. Chem. B* **1999**, *103*, 8817.
(81) Park, E.; Andrews, S.; Boxer, S. G. *J. Phys. Chem.* **1999**, *103*, 9813.
(82) Loring, R. F. Private commication, 2002.
(83) Merchant, K. A.; Noid, W. G.; Thompson, D. E.; Akiyama, R.; Loring, R. F.; Fayer, M. D. **2002**, submitted.